



**HAL**  
open science

## On-line optical absorption of electron-irradiated yttria-stabilized zirconia

Jean-Marc Costantini, Olivier Cavani, Bruno Boizot

► **To cite this version:**

Jean-Marc Costantini, Olivier Cavani, Bruno Boizot. On-line optical absorption of electron-irradiated yttria-stabilized zirconia. *Journal of Physics and Chemistry of Solids*, 2022, 169, pp.110853. cea-04151157

**HAL Id: cea-04151157**

**<https://cea.hal.science/cea-04151157>**

Submitted on 4 Jul 2023

**HAL** is a multi-disciplinary open access archive for the deposit and dissemination of scientific research documents, whether they are published or not. The documents may come from teaching and research institutions in France or abroad, or from public or private research centers.

L'archive ouverte pluridisciplinaire **HAL**, est destinée au dépôt et à la diffusion de documents scientifiques de niveau recherche, publiés ou non, émanant des établissements d'enseignement et de recherche français ou étrangers, des laboratoires publics ou privés.

## ON-LINE OPTICAL ABSORPTION OF ELECTRON-IRRADIATED YTTRIA-STABILIZED ZIRCONIA

Jean-Marc COSTANTINI<sup>1</sup>,

Université Paris-Saclay, CEA, Service de Recherches Métallurgiques Appliquées, 91191, Gif-sur Yvette, Cedex, France

Olivier CAVANI, and Bruno BOIZOT,

Laboratoire des Solides Irradiés, École Polytechnique, 91128 Palaiseau, Cedex, France.

### **ABSTRACT**

The kinetics of color-center formation and decay in electron-irradiated cubic yttria-stabilized zirconia ( $\text{ZrO}_2: \text{Y}^{3+}$ ) is followed by on-line UV-visible absorption spectroscopy. Growth and time decay of absorption spectra was measured upon electron irradiation and subsequent beam shut-off for energies of 0.8, 1.0, 1.75, and 2.5 MeV. For a high beam current intensity, spectra are fitted by two broad absorption bands centered at 3.0 eV and 3.8 eV. Such bands are assigned to the so-called T-center, i. e.  $\text{Zr}^{3+}$  ions in a trigonal point symmetry, which is produced by ionization processes either by photon irradiation or charged particle irradiation. A red-shift of absorption spectra is observed for lower current intensities regardless of electron energy. Such a modification is attributed to a change in the local environment of  $\text{Zr}^{3+}$  ions due to the formation of neighboring oxygen vacancies by elastic collisions, depending on the electron energy and enhanced by a higher flux. A common behavior of increase of the differential absorbance to similar saturation values after accumulation of the irradiation dose and time-decays to similar non-zero asymptotic values are observed, regardless of the electron energy. However, the rise time and lifetime deduced from growth and decay curves of the absorbance are depending on the electron energy. The increase and saturation of the T-center growth rate with electron energy is attributed to competitive channels of hole trapping on the oxygen and zirconium vacancies induced by elastic collisions. The present on-line experiments reveal the complex process of point-defect generation resulting from the interplay of displacement damage and electronic excitations.

**Keywords:** Yttria-stabilized zirconia, electron irradiation, color centers, UV-visible absorption spectroscopy, *in situ* measurements.

---

<sup>1</sup> Corresponding author's email : [jean-marc.costantini@cea.fr](mailto:jean-marc.costantini@cea.fr)

## I. INTRODUCTION

Yttria-stabilized zirconia ( $\text{ZrO}_2: \text{Y}$ ) or YSZ was widely used as a substrate for the growth of high  $T_c$  superconductor epitaxial films [1] and also for catalysis applications [2]. It is also envisioned as a solid oxide fuel cell (SOFC) material [3], owing to its large oxygen deficiency and high ionic conductivity. It is indeed a very good ionic conductor at high temperature with a maximum of conductivity for  $\sim 8$  mol%  $\text{Y}_2\text{O}_3$  [4]. The high-temperature cubic fluorite ( $\text{CaF}_2$ ) structure is stabilized at room temperature for yttria contents above  $\sim 7$  mol% [4]. The substitution of  $\text{Y}^{3+}$  ions ( $\text{Y}_{\text{Zr}'}$ ) for  $\text{Zr}^{4+}$  ions generates oxygen vacancies with the 2+ charge ( $\text{V}_\text{O}^{\bullet\bullet}$ ) by charge compensation [4]. Those vacancies stabilize the cubic structure above a critical concentration value of  $[\text{V}_\text{O}^{\bullet\bullet}] = \frac{1}{2} [\text{Y}_{\text{Zr}'}]$  about 7 at% [4].

YSZ can also be considered as a non-radioactive surrogate of actinide dioxides with the same crystalline structure, such as  $\text{UO}_{2.0}$  for the 4+ oxidation states of U and Zr. Actually, all those dioxides with the fluorite-like structure such as  $\text{UO}_2$  and  $\text{CeO}_2$  are radiation-resistant materials that cannot be amorphized either by accumulation of point defects in atomic collision cascades or by track overlap due to electronic excitations, even for high ion fluences and high stopping powers [5]. The polygonization of YSZ found after irradiation by swift heavy ions [6] is similar to that of urania exposed to fission fragments [7]. Among other oxide materials such as MgO, YSZ is recognized as a potential matrix for minor actinide transmutation in a nuclear reactor [8]. The knowledge of point defect formation in the fluorite-like dioxides such as YSZ is thus a key issue for the nuclear applications.

The damage in YSZ after charged particle or neutron irradiations was extensively studied by various experimental techniques such as transmission electron microscopy [9] X-ray diffraction [5, 10, 11], Rutherford backscattering-channeling spectrometry [9, 11], electron paramagnetic resonance (EPR) spectroscopy [12], and UV-visible absorption spectroscopy [12, 13]. The formation of point defects induced by UV-rays and X-rays was also studied at length [14-18]. Two main types of paramagnetic color centers are found in YSZ after charged particle irradiations: i) the so-called T-centers (or  $\text{Zr}^{3+}$  ions,  $\text{Zr}_{\text{Zr}'}$  in a trigonal point symmetry,  $C_{3v}$ , surrounded by two oxygen vacancies  $\text{V}_\text{O}^{\bullet\bullet}$  along a  $\langle 111 \rangle$  direction) induced by ionization or electronic excitations, and ii)  $\text{F}^+$ -type centers (oxygen divacancies  $[\text{V}_\text{O}^\bullet - \text{V}_\text{O}^{\bullet\bullet}]^\cdot$  or  $\text{F}_2^+$  centers in an axial  $\langle 100 \rangle$  symmetry) induced by elastic collisions or nuclear collisions [5, 19]. The T-center is also formed by single excitations for UV-ray or X-ray irradiations [14-18]. Photo-bleaching and thermal annealing was also studied for those two color centers [20, 21]. Minor paramagnetic hole centers ( $\text{O}_\text{O}^\cdot$ ) such as the neutral oxygen hole centers OHC ( $[\text{Y}_{\text{Zr}'} - \text{O}_\text{O}]^\times$ ) were also detected for photon [15] or charged particle irradiations [21].

The kinetics of growth and decay of color centers was also followed as a function of irradiation time for X-ray irradiation and 2.5-MeV electron irradiation by using EPR spectroscopy and on-line UV-

visible absorption spectroscopy [22]. The aim of the present study is to extend those results by following the growth and time decay of the on-line UV-visible absorbance of YSZ for various electron energies. The present data show a common behavior of point-defect growth to saturation and time decay to non-zero asymptotic values after beam shut-off for all electron energies. The evolution of absorption bands of the color centers and the dependence of their rise time and lifetime on the electron energy is addressed on the basis of combined effects of ionization and elastic collisions.

## II. EXPERIMENTAL PROCEDURES

We have used YSZ single crystal plates (9.5 mol% yttria) of 500  $\mu\text{m}$  in thickness and 10 x 10  $\text{mm}^2$  in size supplied by Crystal GmbH (Berlin, Germany) with low impurity contents [23]. The as-grown crystals were polished on both sides and were transparent and colorless. On-line UV-visible absorption measurements were carried out at the SIRIUS accelerator (Ecole Polytechnique, Palaiseau, France) by using electron energies of 0.8, 1.0, 1.75, and 2.5 MeV [24]. The  $\lambda$  optical spectrometer with a  $\lambda$  detector of  $\lambda$  channels was calibrated with a Hg lamp for each set of experiments. The resolution was of  $\Delta\lambda \sim 0.1\text{-}0.2$  nm for a wavelength of  $\lambda \sim 375$  nm.

The picture of the experimental set-up inside the irradiation chamber is shown in Fig. 1. The target plate was set on an iris of 10 mm in diameter at 45 deg. angle off the electron beam axis and the optical absorption spectrum was collected at 90 deg. off-axis. The irradiated side of the sample was facing the spectrometer (bottom side in Fig. 1) with the light source in the opposite direction (top side in Fig. 1). The electron beam was collimated by a diaphragm of 8 mm in diameter at the entrance of the chamber (left side on Fig. 1). A beam diameter of  $\sim 33$  mm (surface of  $S \sim 8.55$   $\text{cm}^2$ ) was measured on a glass plate mounted on the target holder regardless of electron energy. The beam current was measured with a Faraday cup outside the chamber after crossing the target (right side in Fig. 1). The beam current intensity ( $I$ ) on target was ranging between 0.03  $\mu\text{A}$  and 0.5  $\mu\text{A}$ , i. e. with beam current densities ( $i = I/S$ ) ranging from  $i \sim 0.003$   $\mu\text{A cm}^{-2}$  to  $i \sim 0.06$   $\mu\text{A cm}^{-2}$ , and electron flux ( $\phi = it/e$ ) ranging from  $\phi \sim 2 \times 10^{10}$   $\text{e}^- \text{cm}^{-2} \text{s}^{-1}$  and  $\phi \sim 4 \times 10^{11}$   $\text{e}^- \text{cm}^{-2} \text{s}^{-1}$ .

For each new virgin sample, the “blank” (100 %) transmission spectra and “dark” spectra were recorded before starting the irradiation. The cut-off wavelength of the blank spectrum was of  $\lambda \sim 285$  nm. The spectra were actually recorded versus wavelength between 194 nm and to 462 nm. The integration time of each spectrum was set to values of  $\Delta t = 188$  ms or  $\Delta t = 256$  ms depending on the power of the light source. Smoothing of each spectrum was carried out on 7 pixels. No averaging of spectra was done. The transmission spectra of irradiated samples were recorded in the differential mode with respect to the virgin spectrum and corrected for the dark spectrum. Several scans were then carried out in-beam as a function of time until the spectrum exhibits saturation of the differential

transmittance (T) up to a given irradiation time. The corresponding deposited dose ( $Q = It$ , in C) and irradiation fluence ( $\phi t$ , in  $e^- \text{ cm}^{-2}$ ) can be estimated from the beam current intensity or electron flux and the elapsed irradiation time (t) for each spectrum. Larger doses were of course reached with the larger integration time ( $\Delta t$ ) and beam current intensity (I). Time decay was then followed on-line after beam shut off. The same time step ( $\Delta t$ ) was also used for the sequential recording of spectra. The spectra were processed by plotting the differential absorbance  $A = -\log(T)$  as a function of photon energy in eV. The variation of reflectivity (R) at the air/sample interfaces deriving from change in refractive index (n) of the irradiated samples is overlooked. Reflectivity can be estimated from the standard Fresnel's equation for the normal incidence:  $R = (n - 1)^2 / (n + 1)^2$  giving  $R \sim 13.5\%$  in the visible range for  $n = 2.1585$  for  $\lambda = 500 \text{ nm}$ . The same value is found for the incidence and output angles of 45 deg. and  $R \sim 4.3\%$  for the output angle at 0 deg. These reflectivity losses can anyway be neglected.

The total inelastic stopping power ( $S_{\text{inel}} = -dE/dx$ ) and range of impinging electrons in  $\text{ZrO}_2$  computed with the ESTAR code [25] are displayed in Table 1 for the various energies. The stopping power is almost constant in this electron energy range. For all four energies, the electrons were transmitted through the targets in thickness of 0.5 mm.

### III. RESULTS

The raw absorption spectra are shown for the four electron energies for various doses or irradiation times up to the saturation of the differential absorbance (Figs. 2 a-b-c-d). The colorless samples turned to a yellow color after irradiation corresponding to a maximum absorbance at  $\sim 3.0 \text{ eV}$  ( $\lambda \sim 400 \text{ nm}$ ), i. e. in the blue range. The null differential absorbance value for the virgin sample corresponds to the blank spectrum for  $T = 100\%$ . It is seen that different shapes of absorption spectra are obtained for the 2.5-MeV electrons depending on the beam current intensity. For the high intensities ( $0.5 \mu\text{A}$ ) and high doses, spectra are fitted with two broad Gaussian bands centered at 3.0 eV and 3.8 eV with FWHM of  $\sim 0.7 \text{ eV}$  and  $\sim 1.3 \text{ eV}$ , respectively (Fig. 2 a). The spectra for low beam intensities ( $\sim 0.05 \mu\text{A}$ ) are red-shifted with respect to the higher ones, regardless of the electron energy (Figs. 2 b-c-d). As a result the shapes of spectra look different with a shifted maximum. The deviations of fits near 4.2 eV for all spectra mainly stem from the subtraction of band tailing on the differential absorbance near the fundamental absorption edge of YSZ (band-gap energy of  $E_G = 4.2 \text{ eV}$  for 9.5 mol%  $\text{Y}_2\text{O}_3$ ) [26].

The spectra exhibit a growth of the absorbance up to saturation then decay to the same spectrum after beam shut-off (Fig. 3 a-b-c-d). There is decay to an irreversible absorbance of the sample corresponding to the change in color. The growth of the differential absorbance (A) versus

irradiation time ( $t$ ) for the reference photon energies of 3.0 eV and 3.3 eV is least-square fitted with the saturation function:

$$A = A_s (1 - e^{-t/\tau}) \quad (1)$$

where  $A_s$  is the saturation value, and  $\tau$  is the rise time. A quicker rise is found for higher electron energies. Saturation occurs at about 5 s for 2.5 MeV and 10 s for 0.8 MeV. The time decays of the differential absorbance are shown for the four energies (Figs. 3 a-b-c-d), taken after shutting off the beam for about the same initial absorbance of  $A_0 \sim A_s \sim 0.1$ . They were also taken for the same photon energies of 3.0 eV and 3.3 eV. A faster decay is found for higher electron energy. Good least-square fits of the decay curves (Figs. 3, insets) are obtained with an exponential decay function with non-zero asymptotic values versus decay time ( $t'$ ):

$$A = A_\infty + (A_0 - A_\infty) e^{-t'/\tau'} \quad (2)$$

where  $A_0$  is the initial value of the differential absorbance before beam shut-off,  $A_\infty$  is the asymptotic value, and  $\tau'$  is the lifetime. The asymptotic values are reached in about 10 s. The value of  $A_0 \sim 0.1$  corresponds to a differential absorbance of  $T_0 \sim 80\%$ . Best-fit parameters are reported in Table 1 for the various electron energies. The lifetime and rise time are decreasing with the electron energy for similar  $A_s$  and  $A_0$  values, that are increasing with the electron energy. Similar  $\tau$  and  $\tau'$  values are found at 3.8 eV for the high current intensity with 2.5-MeV electron beams.

#### IV. DISCUSSION

On-line in-beam and off-beam optical absorption measurements allow following the defect formation in solids or liquids. For instance, radiolytic products of water, such as the solvated electron ( $e_{aq}^-$ ), were detected by on-line optical absorption features [27]. In-situ picosecond and femtosecond pump-probe spectroscopy experiments were also applied to study the formation and time decay of color centers in alkali halides, such as NaCl and LiF [28], and binary oxides, such as MgO and SiO<sub>2</sub>, upon pulsed laser irradiation [29]. Transient species, such as the self-trapped exciton (STE), and their evolution were followed on a very short time scale for those oxides [29]. To our knowledge, no such time-resolved experiments were carried out for complex oxides such as YSZ with a large amount of oxygen deficiency.

However, on a much longer time scale, on-line measurements for 2.5-MeV electron irradiation of YSZ have reported the growth of the 3.3-eV absorption band ( $\sim 375$  nm) versus irradiation time up to saturation and sequential time decay after beam shut-off [22]. Both growth and decay data were

least-square fitted with exponential rise or decay curves to asymptotic values like in Eqs. (1)–(2). There is an overall qualitative agreement on the behavior of the absorption bands that can be assigned to the color-center formation by electron irradiation in YSZ. The fitted value of the rise time ( $\tau = 10$  min) and lifetime ( $\tau' = 18$  min) of the 3.3-eV band for 2.5-MeV electrons [22] are larger than the present results, but they lie in the same range. This means that the recombination processes associated to the decay of the associated optical absorption are quite slow as opposed to the fast decay of transient species such as STEs or some hole centers [28-29].

This 3.3-eV band was ascribed to T-center ( $Zr^{3+}$ ) formation by ionization processes with X-rays and swift electrons [14-19, 23]. We have suggested a kinetic rate model for the growth and decay of T-centers upon irradiation [22, 23]. Basically, the model for growth involves trapping of a free electron on  $Zr^{4+}$  ( $Zr_{Zr^x}$ ) lattice sites and subsequent free hole trapping on  $Zr^{3+}$  ( $Zr_{Zr'}$ ) leading to an equilibrium state leading to Eq. (1). For the decay, a similar model yields a non-zero asymptotic value according to Eq. (2). The large values of  $\tau$  and  $\tau'$  found for all energies hint to some slow hopping process of charge transport in this insulating material. The decay rate ( $\propto \tau'^{-1}$ ) is definitely smaller than the growth rate ( $\propto \tau^{-1}$ ) owing to the low mobility of holes with respect to electrons. Within the above-mentioned model, it was established from rate equations that  $\tau^{-1} = \sigma_r \phi$ , where  $\sigma_r$  is the thermally-activated recombination cross section of holes on  $Zr_{Zr^x}$  [22]. Hole trapping is the limiting factor of T-center growth. From the classical free-carrier generation-recombination theory used for semiconductor photoconductivity modeling [30], we can also write that  $\tau^{-1} = n_0 v \sigma_r$ , under steady state conditions, where  $n_0$  is the total concentration of recombination centers, and  $v$  is the mean free-carrier thermal velocity. As a result, it is found that  $\sigma_r$  will vary as  $1/\phi$ , for a given trapping center and given temperature.

However, the shape of the absorption spectra is clearly changed with the beam current intensities. The absorbance at  $\sim 3.8$  eV is increased for higher intensities. Moreover, the dependence of the rise time and lifetime on the electron energy for a similar irradiation time and dose cannot be accounted for by a difference in inelastic stopping power ( $S_{inel}$ ), since it is almost constant in the studied energy range (Table 1).

The  $\tau^{-1}$  and  $\tau'^{-1}$  values for photon energies of 3.0 eV and 3.3 eV are plotted versus electron energy (Fig. 4). The parameters of the absorption band at 3.8 eV for a high flux are close to those two bands (Table 1). It shows an increase of the  $\tau^{-1}$  values (Fig. 4, left scale) as a function of electron energy with an increase at  $\sim 1$  MeV and a saturation above  $\sim 1.5$  MeV according to a sigmoid curve. An almost constant value of  $\tau'^{-1}$  is found up to 1.75 MeV, then a small increase for 2.5 MeV (Fig. 4, left scale). The  $A_s$  value is also increasing versus electron energy regardless of the dose (Table 1) according to a saturation function like Eq. (1) (Fig. 4, left scale). The good agreement between the three bands shows

the consistency of measurements. Moreover, it is seen that the  $\tau'$  value for all bands does not depend on flux for the 2.5-MeV energy, even though the spectrum has a different shape for a higher beam current and a higher dose (Table 1, Fig. 4, left scale). As mentioned above, the  $\tau'^{-1}$  values are clearly lower than  $\tau^{-1}$  values. However such a dependence of those parameters on electron energy does not fit our simple model.

Actually, for increasing electron energy, a large number of  $F^+$ -type centers ( $[V_{O^\bullet} - V_{O^\times}]$  involving paramagnetic oxygen vacancies,  $V_{O^\bullet}$ ) are produced by elastic collisions [5, 19]. EPR data have shown that the threshold displacement energy of oxygen atoms is quite high ( $E_d(O) \sim 120$  eV) in agreement with the Molecular Dynamics (MD) simulations [31]. This likely derives from the high recombination rate of oxygen Frenkel pairs (FPs), owing to the large native oxygen vacancy content  $\sim 10$  at%. However, the absorption band of those  $F^+$ -type centers is centered at about 2.4-2.5 eV at RT with little impact in the photon energy range of the present spectra from 2.7 eV to 4.2 eV. Moreover, MD simulations have also shown that stable Zr FPs can also be generated for  $E_d(Zr) = 80$  eV. The displacement cross section of O atoms ( $\sigma_d(O)$ ) and Zr atoms ( $\sigma_d(Zr)$ ) are computed with the SMOTT/POLY code [32] and plotted in barn units as a function of electron energy (Fig. 4, right scale). The atomic concentration of displaced atoms is given by  $\sigma_d \phi t$  for both atoms. The similar increase of  $\sigma_d$  for both atoms and  $\tau^{-1}$  above  $\sim 1$  MeV is hinting to a possible correlation between the T-center growth rate and vacancy formation. The plot of  $\sigma_d(Zr)$  exhibits a much steeper increase than  $\sigma_d(O)$  as a function of electron energy for  $\sim 1.5$  MeV.

Three broad absorption bands centered at 3.1, 3.45 and 4.05 eV were previously deduced from spectra at 8 K after swift heavy ion irradiations [33]. They showed a similar growth rate with ion fluence and were assigned to the T-centers with a different distortion parameter of the cubal  $D_{3d}$  point symmetry leading to the lower axial  $C_{3v}$  point symmetry. However, no such large shift to 2.6-eV was ever evidenced for the T-center absorption band to our knowledge. Rather, the 2.73-eV band was attributed to oxygen di-vacancies ( $F^+$ -type centers). A possible explanation is a variation of the T-center from the standard  $[V_{O^{\circ\circ}} - Zr_{Zr'} - V_{O^{\circ\circ}}]^{\circ\circ\circ}$  defect produced by X-rays or UV-rays to another charged species, such as for instance  $[V_{O^{\circ\circ}} - Zr_{Zr'}]^{\circ}$ , i. e. the so-called C-center [14, 15], with shifted absorption bands. The latter color center is produced by thermal annealing at high temperature [14, 15]. A band centered at 2.6 eV was actually assigned to those C-centers which do not show any EPR signal. The oxygen vacancies in the local environment of the  $Zr^{3+}$  ions with the  $4d^1$  configuration change the point symmetry and shift the energy levels of the 4d electron split by the crystal field. The spectra may reflect the different contributions of those point defects with a variable local environment of the  $Zr^{3+}$  ions.

An estimation of the T-center concentration ( $N_0$ ) at saturation can be made from the well-known Markham-Smakula's equation for a Gaussian band shape [34]:

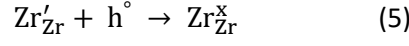
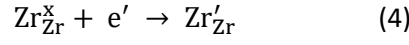
$$N_0 f = 0.87 \times 10^{17} \frac{n}{(n^2 + 2)^2} \alpha_0 W \quad (3)$$

where  $f$  is the oscillator strength of the associated electronic transition,  $W$  is the FWHM of the absorption band in eV, and  $\alpha_0 = 2.3 A_0/t = 4.6 \text{ cm}^{-1}$  is the corresponding absorption coefficient by using the Beer-Lambert's law with an optical path length equal to the sample thickness  $t = 0.05 \text{ cm}$  and for  $A_0 = 0.1$  at the saturation. One finds  $N_0 \sim 8.5 \times 10^{16} \text{ cm}^{-3}$  for  $n = 2.1585$  (for a photon energy of 2.5 eV) and  $W \sim 1 \text{ eV}$  assuming a value of  $f = 0.23$  for the 3.3-eV band, as deduced from combined EPR and optical absorption measurements [33]. For a total atomic density of  $N_a \sim 8.5 \times 10^{22} \text{ cm}^{-3}$ , this yields  $N_0/N_a \sim 1 \times 10^{-6}$ , i. e.  $\sim 1 \text{ at. ppm}$  which is quite low. A larger concentration at saturation ( $1.6 \times 10^{17} \text{ cm}^{-3}$ ) was directly measured by EPR spectroscopy for 2.5-MeV electron irradiation [12]. A closer value to the EPR evaluation can be obtained for a twice larger FWHM, or else the  $f$ -value of 0.23 is likely overestimated. Actually, a lower value of  $f = 0.11$  was deduced for the  $F^+$ -type centers [33].

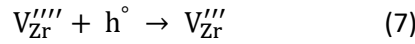
A value of  $f = 0.03$  was indeed obtained for the X-ray induced T-center (with the 3.3-eV absorption band) [17, 18], in agreement with crystal field calculations including a variable distortion parameter ( $\eta$ ) of the  $D_{3d}$  cubal symmetry giving rise to the  $C_{3v}$  axial symmetry along a  $\langle 111 \rangle$  axis. Those low  $f$ -values are consistent with the parity-forbidden electric dipole transitions between crystal field levels for the  $4d^1$  configuration of  $Zr^{3+}$  ions, according to Laporte's rules. The large FWHM of  $\sim 1.6 \text{ eV}$  of the 3.3-eV absorption band was accounted for by a distribution of  $\eta$  values corresponding to different relaxed positions of the oxygen atoms near the two neighboring oxygen vacancies for T-centers [17, 18]. The large FWHM (1.4 eV) of the 2.6-eV band of C-centers can also be ascribed to such relaxation for a single vacancy [15]. It is to be noted that the absorption bands of T-centers, as well as the  $F^+$ -type centers, are insensitive to temperature since the band-width is dominated by the static disorder or not by phonon generation [12, 17].

On the basis of the present experimental results, it turns out that the rate equations used for point-defect growth and decay must be revisited by including extra bodies, i. e. the vacancies induced by the irradiation. It is actually seen that  $\sigma_d(O)$  and  $\tau^{-1}$  are both increasing versus electron energy with a similar rate (Fig. 4). Obviously, oxygen vacancy formation is enhancing the T-center growth. This is consistent with the increase of  $A_s$  and  $A_0$  values with electron energy regardless of the irradiation dose (Table 1, Fig. 4 left scale). The increase of absorbance near 3.8 eV for a larger beam current must also be considered. However, the  $\tau$  and  $\tau'$  values at 3.8-eV are close to those at 3.0-eV and 3.3-eV for the 2.5-MeV electrons (Table 1). As a result, no clear flux effect is found on those parameters even though the spectra look different.

As mentioned above in the previous simple model, we have considered the two following reactions of trapping of the free electrons and free holes generated by above band-gap excitations:

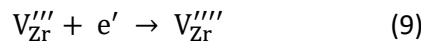


By solving the corresponding rate equations, we have concluded that hole trapping on  $\text{Zr}'_{\text{Zr}}$  is the limiting factor of T-center growth [22, 23]. This yields that  $\tau^{-1} = \sigma_r \varphi \sim k'$ , where  $k'$  is the rate constant of reaction (5). Hole trapping onto oxygen ( $\text{O}_\text{O}^{\times}$ ) lattice ions (or  $\text{Y}_{\text{Zr}'}$  sites) could also lead to hole-center formation. However, those native trapping sites bear no relationship with the electron irradiation. Therefore, the increase of the growth rate with electron energy is likely related to point-defect formation. Indeed, trapping of free holes on the O and Zr vacancies can limit the trapping on the  $\text{Zr}'_{\text{Zr}}$  sites, according to the following competitive reactions:



Further channels of trapping holes may be possible on the Zr vacancies, such as  $\text{V}'_{\text{Zr}}$ , thereby stabilizing those highly charged vacancies with large formation energies [35, 36]. It is to be noted that the five charge states of  $\text{V}_{\text{Zr}}$  (-4, -3, -2, -1, 0) have a similar high formation energy depending on the Fermi level position [35, 36].

In addition, the following free-electron trapping reaction on the Zr and native O vacancies must also be taken into account:



The concentrations of  $\text{V}_\text{O}^{\circ}$  and  $\text{V}'_{\text{Zr}}$  are increasing with electron energy owing to the increase of  $\sigma_d$  for both atoms (Fig. 4, right scale). Since  $[\text{V}_\text{O}^{\circ\circ}] = \frac{1}{2} [\text{Y}_{\text{Zr}'}] = \text{Constant}$ , the reactions (6) and (8) may be overlooked in the steady-state conditions, i. e. for  $\frac{d[e']}{dt} = -\frac{d[h^{\circ}]}{dt} = 0$ , where brackets denote concentration, in the intrinsic case for which  $[e'] [h^{\circ}] = C$ , where  $C$  is a constant depending  $E_G$ .

Calculations show that  $V_O^\circ$  would be unstable with respect to  $V_O^{\circ\circ}$  and  $V_O^x$  due to a negative Hubbard U effect [35]. As a result, hole trapping may also occur on  $V_O^x$  in equilibrium conditions. However, such equilibrium can be ruled out in the in-beam steady-state conditions for which there is a constant input of oxygen vacancies into the solid.

It is seen that oxygen vacancy formation by irradiation is dominant up to  $\sim 1.5$  MeV (Fig. 4). The saturation of  $\tau^{-1}$  above 1.5-MeV is likely arising from the equilibrium between those reactions under in-beam steady-state conditions. It is striking to notice that saturation takes place at the crossing point between the  $\sigma_d(O)$  and  $\sigma_d(Zr)$  curves, i. e. for an equal number of Zr and O vacancies. However, a quantitative analysis of the kinetics based on rate equations is a complex issue due to the number of reactions involved in the defect formation process.

A more simple approach was used for the analysis of cathodoluminescence of YSZ for high-energy electrons from 0.4 to 1.25 MeV [37]. The rate equations featured the competition between free-electron and free-hole trapping on a single trapping level corresponding to the  $F^+$  center ( $V_O^\circ$ ). However, the trapping cross section of holes ( $\sigma_{t,p}$ ) is likely much lower than that of electrons ( $\sigma_{t,n}$ ). For example,  $\sigma_{t,p} = 3.9 \times 10^{-16} \text{ cm}^2$  for hole capture on defects in  $\text{SiO}_2$ , which is independent of the electric field [38], whereas  $\sigma_{t,n}$  for trapping on  $V_O^\circ$  is ranging between  $10^{-15}$  and  $10^{-13} \text{ cm}^2$  in  $\text{SiO}_2$  [39] and  $\sigma_{t,n} = 2.6 \times 10^{-14} \text{ cm}^2$  in  $\text{ZnO}$  [40] as deduced from DLTS or photo-conductivity data. An estimate of  $\sigma_{t,p}$  for  $Zr^{3+}$  ( $Zr_{Zr}'$ ) ions can also be derived from data of doped n-type or p-type semiconductors, since those charged defects can be considered as  $Zr_{Zr}^x/Zr_{Zr}'$  impurity levels in the band gap of YSZ. Typical values for doped Si range between  $10^{-15}$  and  $10^{-14} \text{ cm}^2$  for  $\sigma_{t,n}$  and between  $10^{-16}$  and  $10^{-15} \text{ cm}^2$  for  $\sigma_{t,p}$  at RT in the cases of dopants such as Mo [41] and Pt [42]. The ratio of electron to hole capture rates or capture cross sections is of  $\sim 40$  for Ni-doped Ge [43] and Ti-doped Si at RT [44]. Hole trapping cross section on  $Zr_{Zr}'$  is most probably as low as for those various dopants. We thus surmise that reactions (5), (6), (8) and (9) can be neglected in a first approximation. Therefore, it turns out that hole trapping on  $V_{Zr}''''$  according to reaction (7) and electron trapping on  $Zr_{Zr}^x$  according to reaction (4) seem the most likely channels.

According to the mass-action law, the equilibrium for those reactions yields:

$$\frac{[V_{Zr}''''][h^\circ]}{[V_{Zr}''']} = K_7 \quad (10)$$

$$\frac{[Zr_{Zr}^x][e']}{[Zr_{Zr}']} = K_4 \quad (11)$$

where  $K_4$  and  $K_7$  are the respective equilibrium constants of reactions (4) and (7). Some simple algebra gives:

$$[Zr'_{Zr}] = \frac{C [Zr^x_{Zr}] [V'''_{Zr}]}{K_2 K_4 [V'''_{Zr}]} \quad (12)$$

This shows that the T-center concentration increases with the Zr vacancy concentration, thereby  $\tau^{-1}$  increases with the electron energy. Such an increase is limited by electron trapping on  $V'''_{Zr}$  according to reaction (9) and hole trapping on  $Zr'_{Zr}$  ( $Zr^{3+}$ ) according to reaction (5) since the capture cross sections are low, yet non null. Considering the mass-action law for reaction (5) with constant  $K_5$ , gives:

$$\frac{[Zr'_{Zr}] [h^\circ]}{[Zr^x_{Zr}]} = K_5 \quad (13)$$

Assuming that  $[e'] = [h^\circ] = C^{1/2}$  in equilibrium conditions, it comes from Eqs. (12)-(13) with simple algebra that a saturation takes place for a ratio depending on reaction (9):

$$\frac{V'''_{Zr}}{V'''_{Zr}} = \frac{K_2 K_4 K_5}{C^{3/2}} \quad (14)$$

Regarding the decay rates, the previous model has shown that it involves both reactions (4) and (5), i. e.  $\tau^{-1} = k + k'$ , where  $k$  is the rate constant of reaction (4), by assuming an equilibrium between the free electrons and T-centers [22, 23]. In the present data, a rather small increase is found for the 2.5-MeV energy (Fig. 4, left scale). Like for the hole trapping reactions, there is an increase of  $\tau^{-1}$  but with a competition between reactions (4) and (9), thereby limiting the increase of the rate constant  $k$ .

## V. CONCLUSION

We have used on-line UV-visible absorption spectroscopy to study the growth and time-decay of color centers in yttria-stabilized zirconia under electron beam. The differential absorbance induced by electrons of 0.8, 1.0, 1.75, and 2.5 MeV was followed in-beam as a function of irradiation time and of decay time after beam shut off. The absorbance centered near 3.3 eV is assigned to the formation of T-centers (i. e.  $Zr^{3+}$  ions in a trigonal point symmetry) by electronic excitations. High beam current intensities induce an increase of absorbance near 3.8 eV which is interpreted by a modification of the local environment with neighboring oxygen vacancies. The rise time is deduced from the growth curves showing saturation and the lifetime from the exponential decay curves to non-zero asymptotic values. Both characteristic times increase with electron energy. The dependence on electron energy is

assigned to the contribution of oxygen and zirconium vacancies induced by elastic collisions to the T-center formation process.

**Acknowledgements:** The authors thank the French EMIR network for supporting this research program.

**Table 1:** Total inelastic stopping power ( $S_{\text{inel}}$ ) and range of electrons in  $\text{ZrO}_2$  (mass density of  $5.81 \text{ g cm}^{-3}$  and mean ionization energy of 294.9 eV) for the various electron energies (E) computed with the ESTAR code [25]. Fitting parameters of the growth and decay curves versus time of the differential absorbance of YSZ at 3.0-eV, 3.3 eV and 3.8 eV: saturation value of growth ( $A_s$ ), and rise time ( $\tau$ ), up to a saturation charge of  $Q_s$ ; initial value before beam shut-off ( $A_0$ ), asymptotic value ( $A_\infty$ ), and lifetime ( $\tau'$ ). The beam current intensity (I) during growth of absorbance prior to time decay is also given.

E (MeV)	0.8	1.0	1.75	2.5	2.5
$S_{\text{inel}}$ (MeV $\mu\text{m}^{-1}$ )	$7.82 \times 10^{-4}$	$7.77 \times 10^{-4}$	$7.98 \times 10^{-4}$	$8.12 \times 10^{-4}$	$8.12 \times 10^{-4}$
Range (mm)	0.82	1.08	2.03	2.95	2.95
I ( $\mu\text{A}$ )	0.03	0.03	0.04	0.06	0.17
$Q_s$ ( $\mu\text{C}$ )	2	15	4	6	36
$A_s$ (3.0 eV)	0.0660	0.0796	0.1141	0.1209	0.1191
$\tau$ (s) (3.0 eV)	5.02	4.43	2.26	2.13	2.41
$A_s$ (3.3 eV)	0.0556	0.0696	0.0950	0.1030	0.1196
$\tau$ (s) (3.3 eV)	5.05	4.62	2.16	2.32	2.69
$A_s$ (3.8 eV)	/	/	/	/	0.0942
$\tau$ (s) (3.8 eV)	/	/	/	/	3.07
$A_0$ (3.0 eV)	0.0655	0.0806	0.0931	0.100	0.120
$A_0$ (3.3 eV)	0.0561	0.0686	0.0795	0.0873	0.121
$A_0$ (3.8 eV)	/	/	/	/	0.0945
$A_\infty$ (3.0 eV)	0.0297	0.0445	0.0520	0.0449	0.0833
$A_\infty$ (3.3 eV)	0.0276	0.0393	0.0488	0.0436	0.0924
$A_\infty$ (3.8 eV)	/	/	/	/	0.0739
$\tau'$ (s) (3.0 eV)	13.77	7.81	8.95	6.12	6.78
$\tau'$ (s) (3.3 eV)	10.32	8.55	8.49	4.85	5.14
$\tau'$ (s) (3.8 eV)	/	/	/	/	6.82

## **REFERENCES**

- [1] P. Pahlke, M. Hering, M. Sieger, M. Lao, M. Eisterer, A. Usoskin, J. Strömer, B. Holzapfel, L. Schultz, and R. Hühne, Thick High  $J_c$  YBCO Films on ABAD-YSZ Templates, *IEEE Trans. on Appl. Supercond.* **25** (2015) 6603804
- [2] M. N. Tsampas, F. M. Sapountzi, and P. Vernoux, Applications of yttria-stabilized zirconia (YSZ) in catalysis, *Catalysis Sci. and Technol.* **1-3** (2015) 1
- [3] S. Hussain, and L. Yangping, Review of solid oxide fuel cell materials: cathode, anode, and electrolyte, *Energy Trans.* **4** (2020) 113
- [4] T. H. Etsell, and S. N. Flengas, The electrical properties of solid oxide electrolytes, *Chem. Rev.* **70** (1970) 339
- [5] J.-M. Costantini, F. Beuneu, and W. J. Weber, Radiation Damage in Cubic-Stabilized Zirconia and Ceria, in *Properties of Fluorite Structure Materials*, Eds. P. Vajda and J. M. Costantini (Nova Science Publishers, New York, 2013), pp. 127-152
- [6] J.-M. Costantini, F. Guillet, S. Lambert, D. Gréville, F. Beuneu, and C. Trautmann, X-ray diffraction study of the damage induced in yttria-stabilized zirconia by swift heavy ion irradiations, *J. Appl. Phys.* **104** (2008) 073504
- [7] H. Xiao, C. Long, and H. Chen, The formation mechanisms of high burnup structure in  $UO_2$  fuel *J. Nucl. Mater.* **556** (2021) 47
- [8] H. Matzke, V. V. Rondinella, T. Wiss, Materials research on inert matrices: a screening study, *J. Nucl. Mater.* **274** (1999) 153151
- [9] S. Moll, L. Thomé, L. Vincent, F. Garrido, G. Sattonnay, T. Thomé, J. Jagielski, and J. M. Costantini, Damage induced by electronic excitation in ion-irradiated yttria-stabilized Zirconia, *J. Appl. Phys.* **105** (2009) 023512
- [10] J. Cheng, and F. B. Prinz, Damage in yttria-stabilized zirconia by Xe irradiation measured by X-ray diffraction, *Nucl. Instrum. Methods B* **227** (2005) 577
- [11] A. Debelle, J. Channagiri, L. Thomé, B. Décamps, A. Boule, S. Moll, F. Garrido, M. Behar, and J. Jagielski, Comprehensive study of the effect of the irradiation temperature on the behavior of cubic zirconia, *J. Appl. Phys.* **115** (2014) 183504
- [12] J.-M. Costantini, F. Beuneu, D. Gourier, C. Trautmann, G. Calas, and M. Toulemonde, Colour centre production in yttria-stabilized zirconia by swift charged particle irradiations, *J. Phys.: Condens. Matter* **16** (2004) 3957

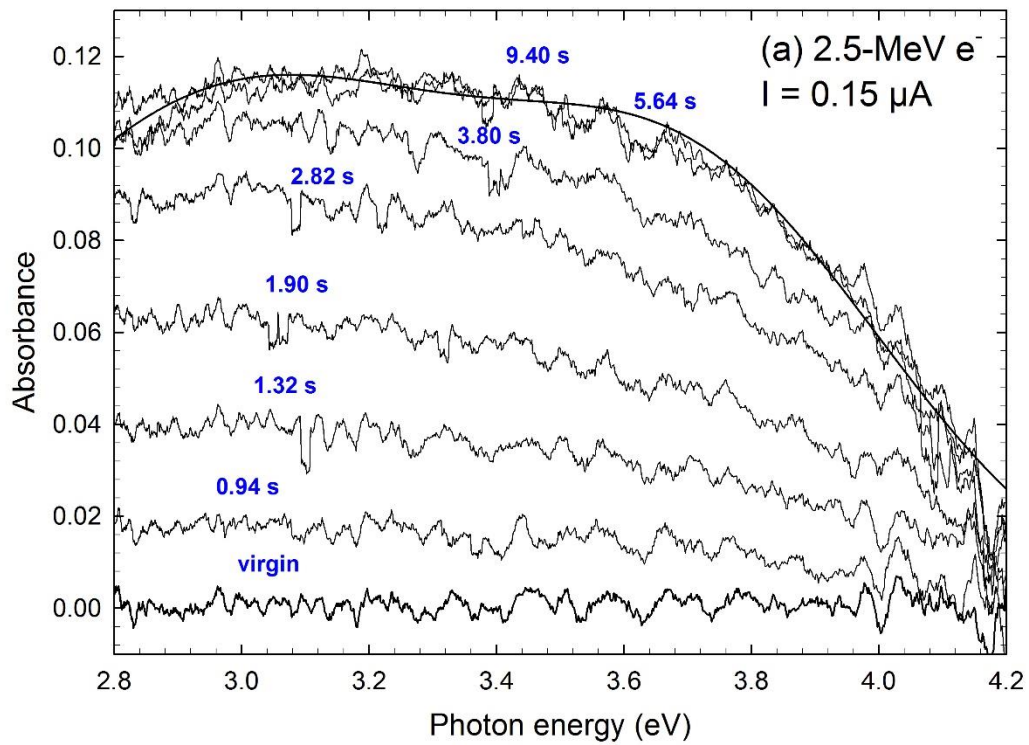
- [13] B. Savoini, D. Caceres, I. Vergara, R. Gonzales, and J. E. Munoz-Santiuste, Radiation damage in neutron-irradiated yttria-stabilized-zirconia single crystals, *J. Nucl. Mater. B* **277** (2000) 199
- [14] V. M. Orera, R. I. Merino, Y. Chen, R. Cases, and P. J. Alonso, Intrinsic electron and hole defects in stabilized zirconia single crystals, *Phys. Rev. B* **42** (1990) 9782
- [15] V. M. Orera, R. I. Merino, Y. Chen, R. Cases, and P. J. Alonso, Electron and hole trapped defects produced by thermoreduction or irradiation in stabilized zirconia, *Radiat. Effects and Defects in Solids* **119-121** (1991) 907
- [16] C. B. Azzoni, and A. Paleari, Sevenfold- and sixfold-coordinated  $Zr^{3+}$  ions in cubic stabilized zirconia: Crystal-field approach, *Phys. Rev. B* **44** (1991) 6858
- [17] C. B. Azzoni, L. Bolis, A. Paleari, G. Scamoggia, and F. Scardina, Disorder-induced optical and paramagnetic properties in zirconium dioxide: Role of low-symmetry crystal fields, *Phys. Rev. B* **51** (1995) 15942
- [18] C. B. Azzoni, L. Bolis, P. Camagni, G. C. Campagnoli, and M. De Simone, A defect model for the optical and EPR activity of the T-center in yttrium-stabilized zirconia, *Radiat. Effects and Defects in Solids* **134** (1995) 485
- [19] J.-M. Costantini, and F. Beuneu, Point defects induced in yttria-stabilized zirconia by electron and swift heavy ion irradiations, *J. Phys.: Condens. Matter* **23** (2011) 115902
- [20] J.-M. Costantini, N. Touati, L. Binet, G. Lelong, M. Guillaumet, and F. Beuneu, Colour centre recovery in yttria-stabilised zirconia: photoinduced versus thermal processes, *Philos. Mag.* **98** (2018) 1241
- [21] J.-M. Costantini, F. Beuneu, and W. J. Weber, Annealing of paramagnetic centres in electron- and ion-irradiated yttria-stabilized zirconia: effect of yttria content, *Philos. Mag.* **94** (2014) 2281
- [22] J.-M. Costantini, M. Fasoli, F. Beuneu, and B. Boizot, Colour centre production in yttria-stabilized zirconia by X-ray and electron irradiations: effect of yttria content, *Philos. Mag.* **94** (2014) 4053
- [23] J.-M. Costantini, and F. Beuneu, Paramagnetic trigonal center production in yttria-stabilized zirconia by electronic excitations, *Nucl. Instr. and Meth.* **314** (2013) 130
- [24] <https://portail.polytechnique.edu/lis/fr/equipements/linstallation-sirius>
- [25] *Stopping Powers for Electrons and Positrons*, International Commission on Radiation Units and Measurements ICRU Report 37 (1984). <https://physics.nist.gov/PhysRefData/Star/Text/method.html>
- [26] P. Camagni, P. Galinetto, G. Samoggia, N. Zema, Optical properties of cubic stabilized zirconia, *Solid State Commun.* **83** (1992) 943
- [27] Y. Du, E. Price, D. M. Bartels, Solvated electron spectrum in supercooled water and ice, *Chem. Phys. Lett.* **438** (2007) 234
- [28] K. S. Song, and R. T. Williams, *Self-trapped excitons* (Springer, Berlin, 1996)

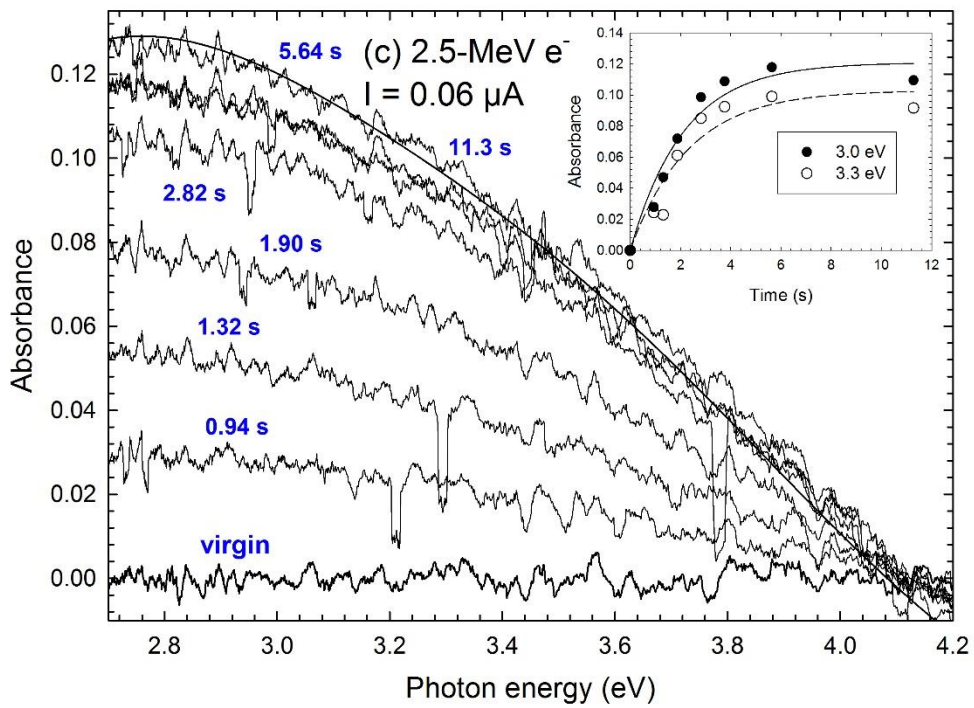
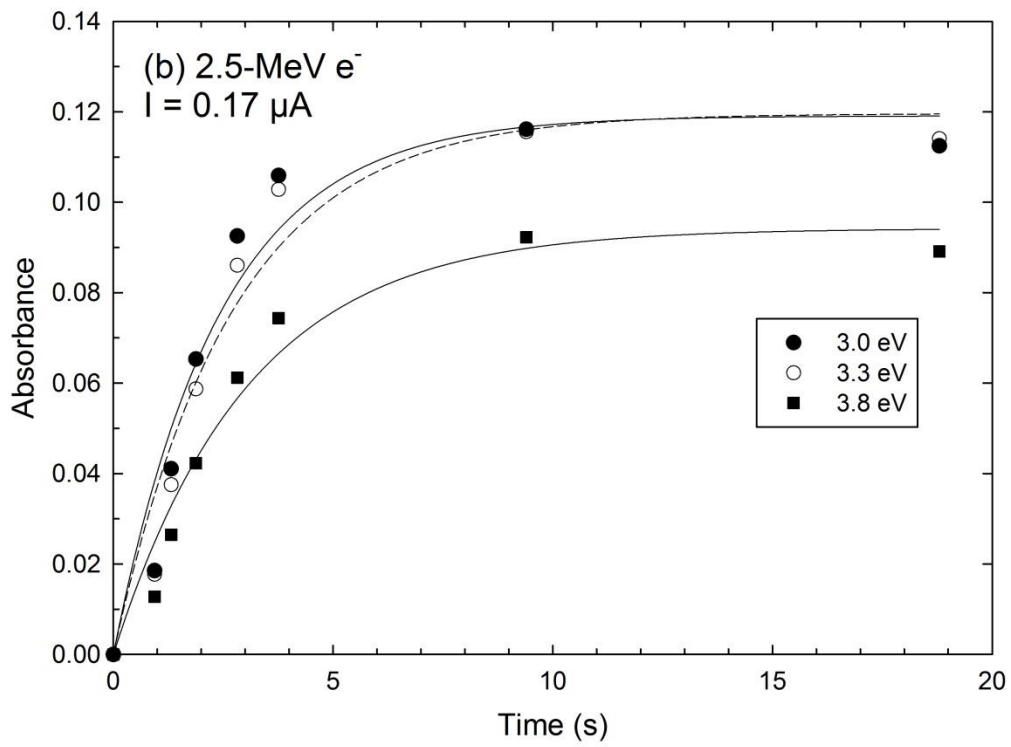
- [29] S. Guizard, P. D'Oliveira, P. Daguzan, P. Martin, P. Meynadier, and G. Petite, Time-resolved studies of carriers dynamics in wide band gap materials, *Nucl. Instr. and Meth. B* **116** (1996) 43
- [30] K. Seeger, *Semiconductor Physics*, Solid-State Sciences, 40, Springer, Berlin, 1991. Chapter 12.
- [31] J.-M. Costantini, F. Beuneu, S. Morrison-Smith, R. Devanathan, and W. J. Weber, Paramagnetic defects in electron-irradiated yttria-stabilized zirconia: Effect of yttria content, *J. Appl. Phys.* **110** (2011) 123506
- [32] D. Lesueur, *Philos. Mag. A* **44** (1981) 905
- [33] J.-M. Costantini, F. Beuneu, K. Schwartz, and C. Trautmann, Generation of colour centres in yttria-stabilized zirconia by heavy ion irradiations in the GeV range, *J. Phys.: Condens. Matter* **22** (2010) 315402
- [34] J. J. Markham, *F-Centers in Alkali Halides* (New York, Academic, 1966)
- [35] J. X. Zheng, G. Ceder, T. Maxisch, W. K. Chim, and W. K. Choi, First-principles study of native point defects in hafnia and zirconia, *Phys. Rev. B* **75** (2007) 104112
- [36] O. I. Malyi, P. Wu, V. V. Kulish, K. Bai, Z. Chen, Formation and migration of oxygen and zirconium vacancies in cubic zirconia and zirconium oxysulfide, *Solid State Ionics* **212** (2012) 117
- [37] J.-M. Costantini, T. Ogawa, A. K. S. I. Bhuian, K. Yasuda, Cathodoluminescence induced in oxides by high-energy electrons: Effects of beam flux, electron energy, and temperature, *J. Lumin.* **208** (2019) 108
- [38] X. Gao, and S. S. Vee, Hole capture cross section and emission coefficient of defect centers related to high-field positive charges in SiO<sub>2</sub> layers, *Solid-State Electron.* **39** (1996) 399
- [39] S. E. Thompson, and T. Nishida, Positive charge generation in SiO<sub>2</sub> by electron-impact emission of trapped electrons, *J. Appl. Phys.* **72** (1992) 4683
- [40] J. C. Simpson, and J. F. Cordaro, Characterization of deep levels in zinc oxide, *J. Appl. Phys.* **65** (1988) 178
- [41] B. B. Paudyal, K. R. McIntosh, D. H. McDonald, and G. Coletti, Temperature dependent carrier lifetime studies on Mo in crystalline silicon *J. Appl. Phys.* **107** (2010) 054511
- [42] S. D. Brotherson, and J. E. Lowther, Electron and hole capture at Au and Pt centers in silicon, *Phys. Rev. Lett.* **44** (1980) 606
- [43] H. F. Tseng, and S. S. Li, Determination of electron and hole capture rates in nickel-doped germanium using photomagnetolectric and photoconductive methods, *Phys. Rev. B* **6** (1972) 3066
- [44] B. B. Paudyal, K. R. McIntosh, and D. H. McDonald, Temperature dependent carrier lifetime studies on Ti-doped multicrystalline silicon, *J. Appl. Phys.* **105** (2009) 124510

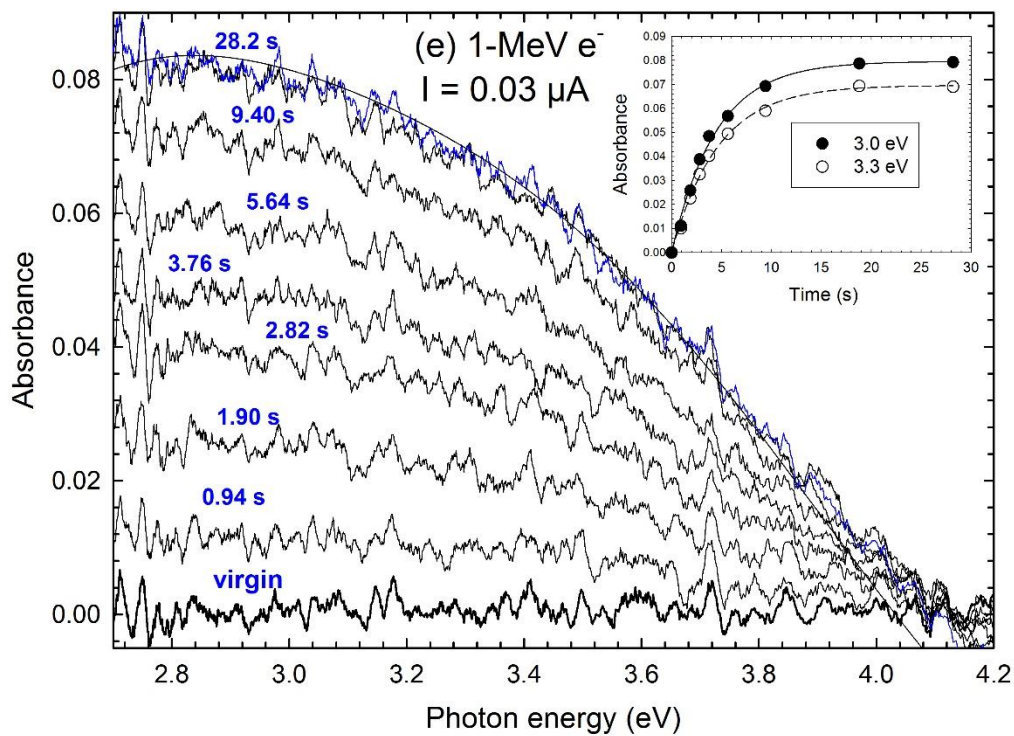
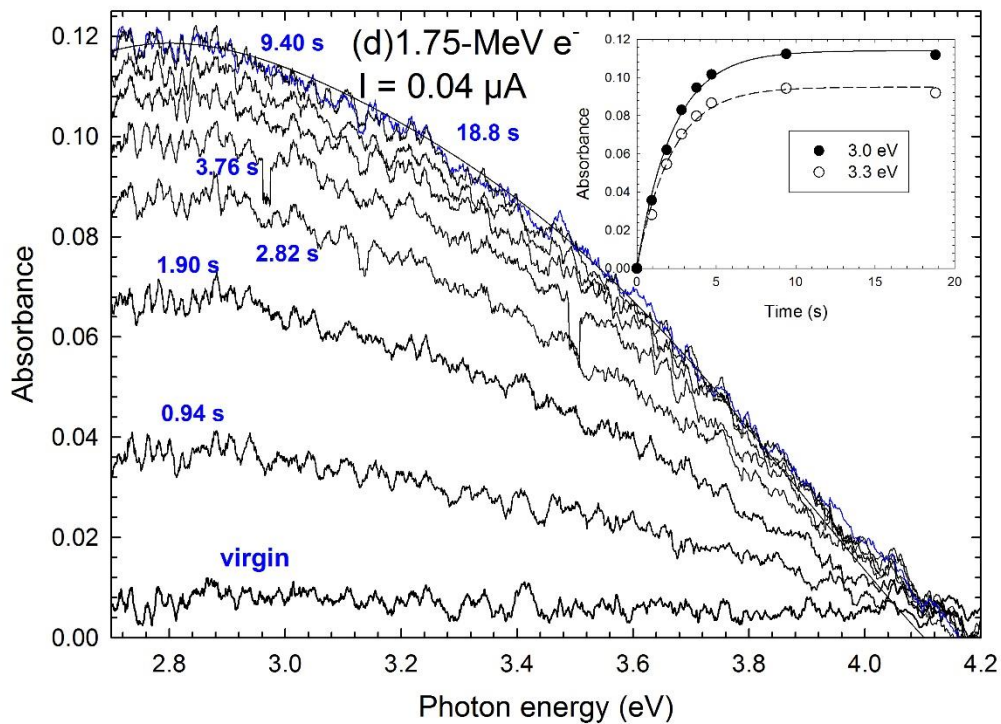
**Figure 1:** Picture of the experimental set-up: the electron beam entrance port of the irradiation chamber is on the left side with the diaphragm of 0.8 mm in diameter, the target sample is mounted at the center of the chamber at 45 deg. off-axis. The optical absorption measurements are carried out at 90 deg. off-axis.

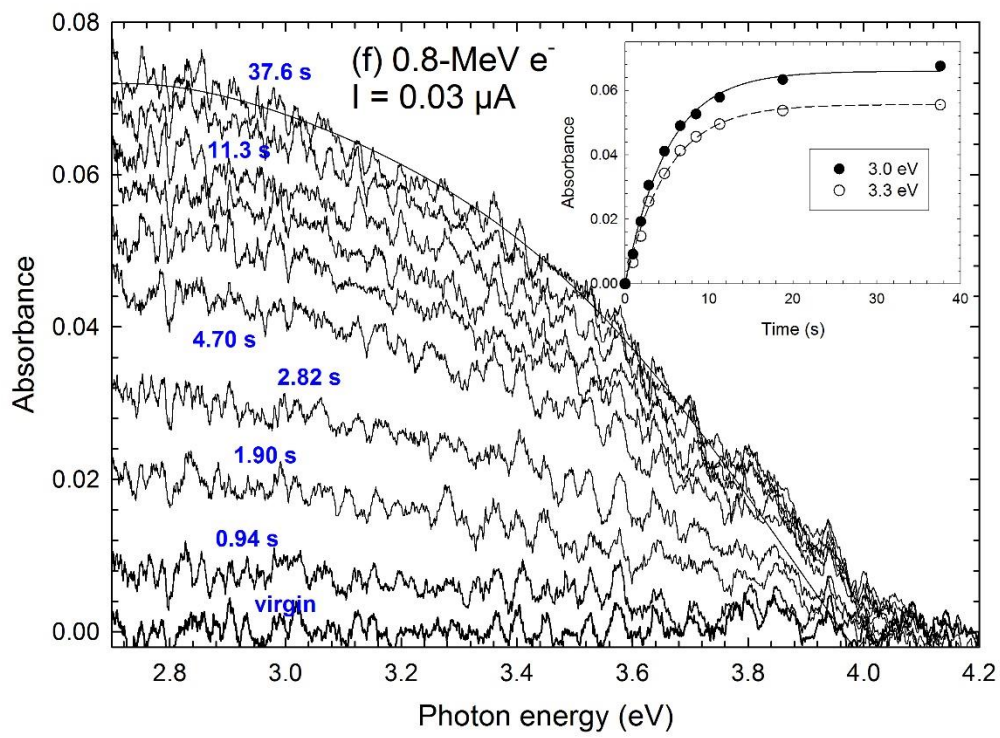


**Figure 2:** UV-visible absorption spectra of YSZ single crystal at RT: in-beam spectra for various irradiation times and various electron energies: 2.5 MeV (a, c), 1.75 MeV (d), 1.0 MeV (e), and 0.8 MeV (f). Solid lines are fits using Gaussian profiles. Growth curves versus irradiation time for 2.5-MeV electrons (b). Insets: Growth curves versus irradiation time; solid and dashed curves are least-square fits with Eq. (1).

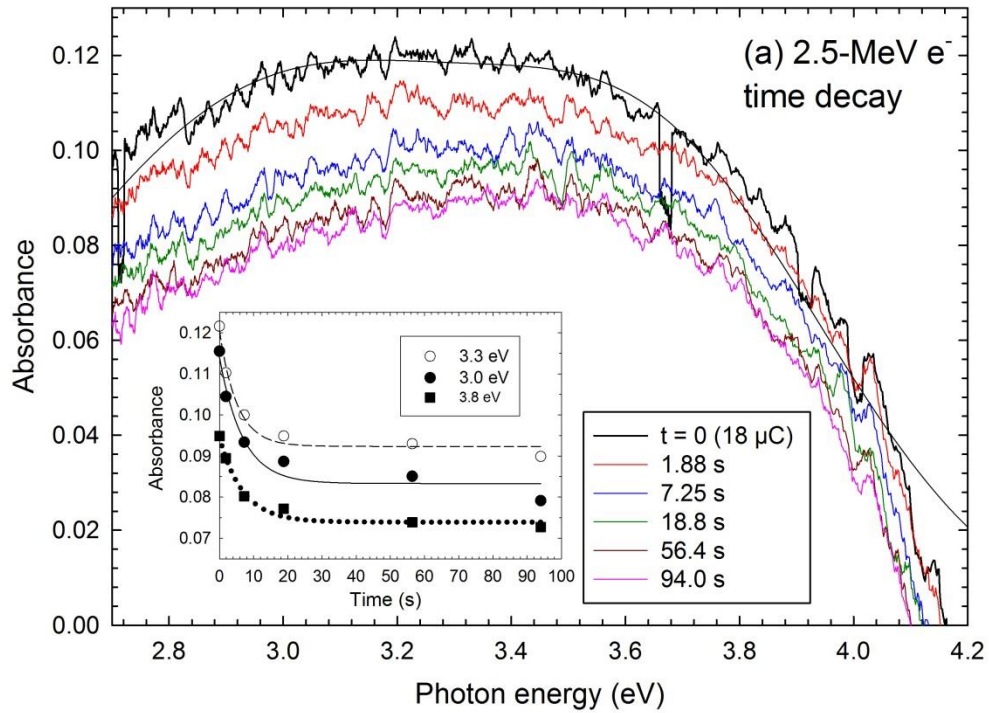


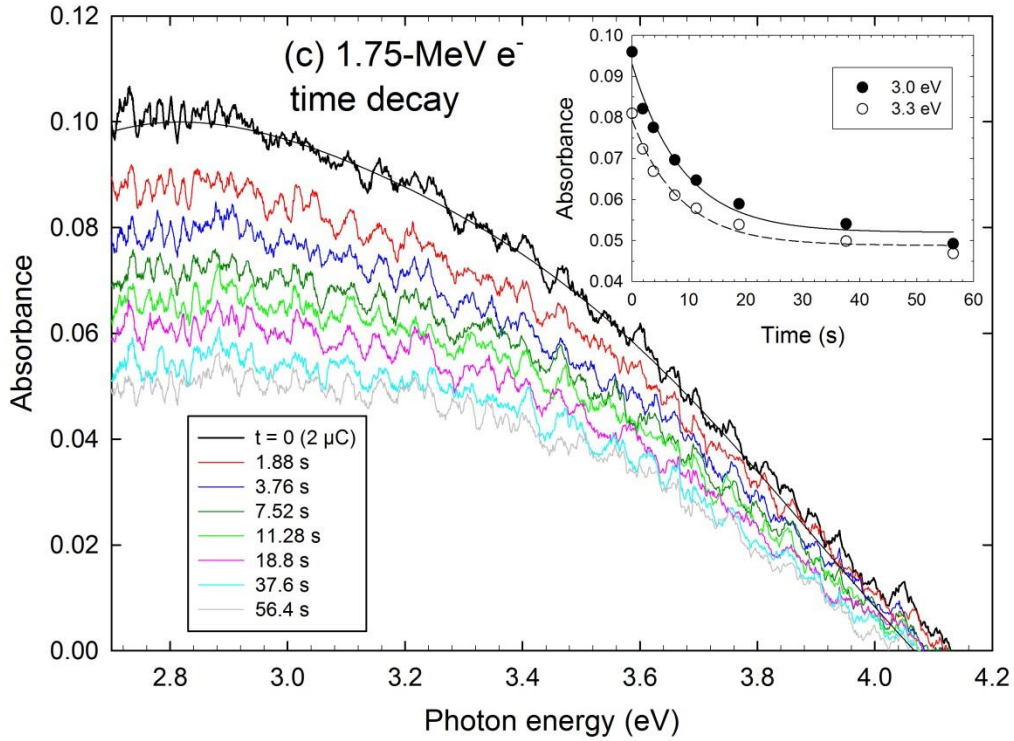
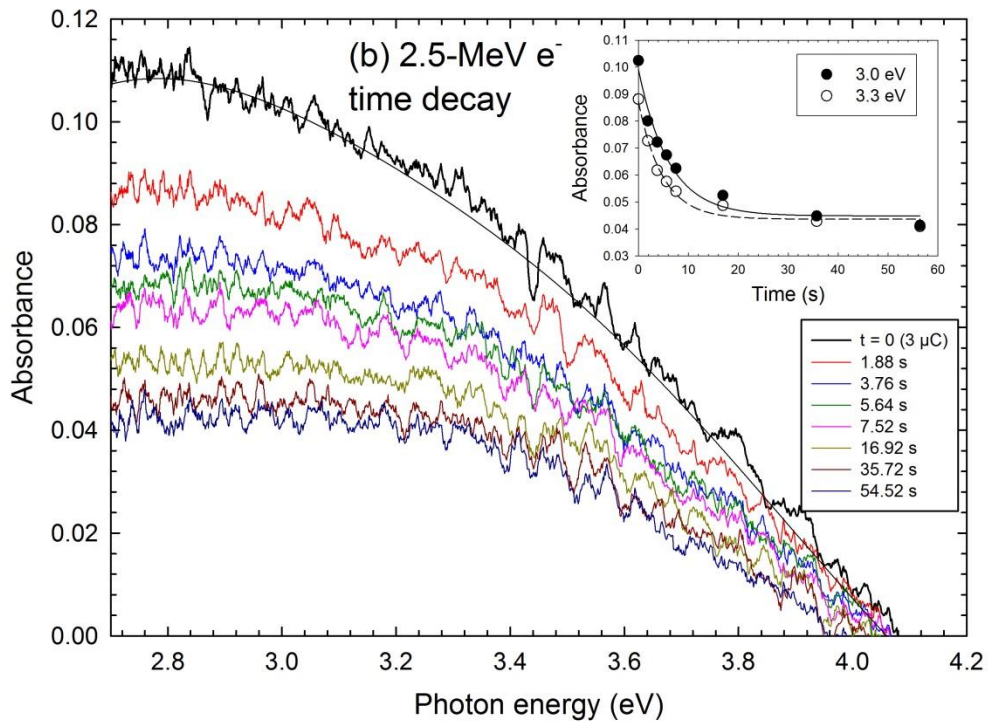






**Figure 3:** UV-visible absorption spectra of YSZ single crystal at RT: off-beam spectra after irradiation for various electron energies: 2.5 MeV (a, b), 1.75 MeV (c), 1.0 MeV (d), and 0.8 MeV (e), as a function of decay time. Solid lines are fits using Gaussian profiles. Insets: Decay curves versus time; solid and dashed curves are least-square fits with Eq. (2).





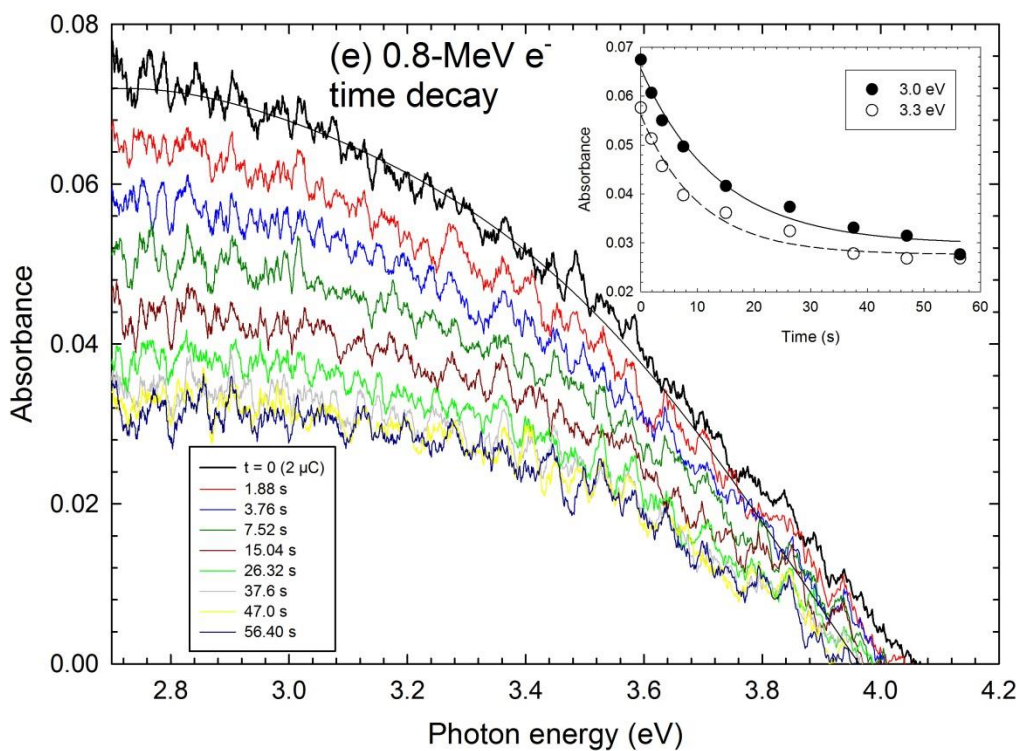
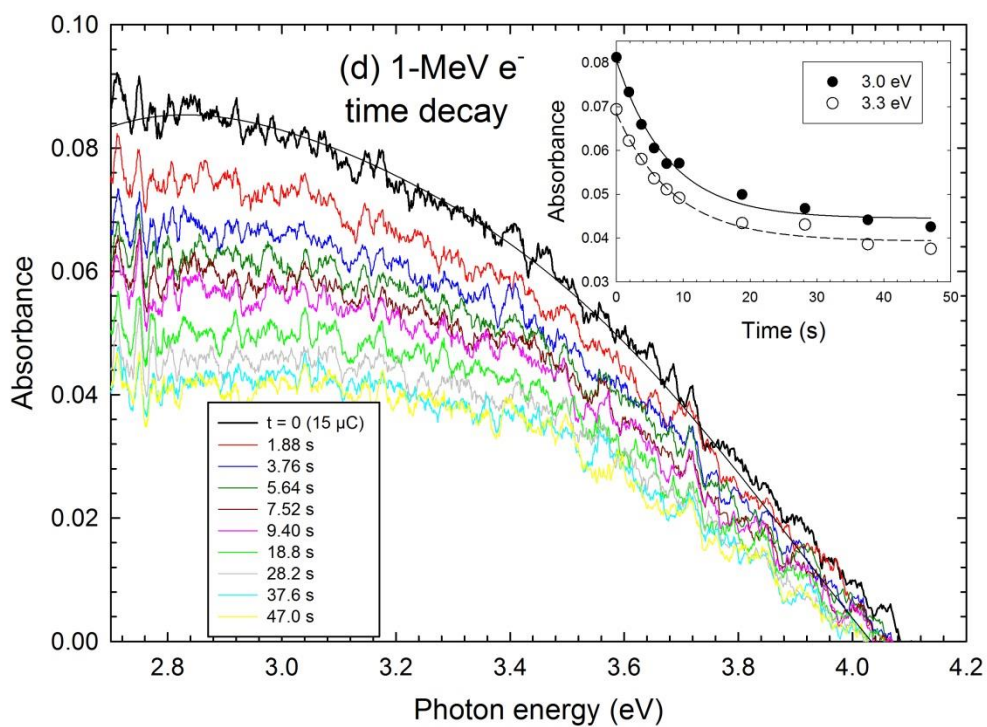


**Figure 4:** Growth rate ( $\tau^{-1}$ ), decay rate ( $\tau'^{-1}$ ), and saturation absorbance ( $A_s$ ) with X 4 magnification (left scale), and displacement cross sections ( $\sigma_d$ ) for Zr and O atoms (right scale), for threshold displacement energies of  $E_d(\text{Zr}) = 80$  eV and  $E_d(\text{O}) = 120$  eV, as a function of electron energy.

